



Synthesis and suitability characterization of microcrystalline cellulose from *Citrus x sinensis* sweet orange peel fruit waste-based biomass for polymer composite applications

Murugesan Palaniappan¹ · Sivasubramanian Palanisamy² · Rashid Khan¹ · Nashmi H. Alrasheedi¹ · Srinivas Tadepalli³ · Thulasi mani Murugesan⁴ · Carlo Santulli⁵

Received: 12 January 2024 / Accepted: 5 March 2024 / Published online: 19 March 2024

© The Polymer Society, Taipei 2024

Abstract

Presently, waste management is the primary focus of scientific inquiry. The recyclable and reusable organic waste are dumped a lot as landfills in the environment and that could be converted into application-oriented polymer reinforcing material. Cellulose is a widespread biopolymer that is found in the majority of bio waste materials. The organic waste *Citrus x sinensis* peel (*Citrus x aurantium* f. *aurantium*) is used as a raw material in this research. The waste material was utilized to extract the cellulose using optimum chemical conditions such as alkali treatment, acid hydrolysis, and bleaching and purification process. Fourier transform spectroscopy was applied to the cellulose to detect the functional groups it contained and indicated progressive removal of non-cellulosic constituents. The cellulose that was extracted has a yield percentage of 67.82% and a density of 1.413 g/cm³. The differential scanning curve analysis reveals that the temperature of degradation is 308.17 °C. Through the utilisation of thermogravimetric analysis, each phase of thermal activity was studied. According to an X-ray diffraction investigation, cellulose has a crystalline size of 9.63 nm and a higher crystallinity index of 72.54 percent exhibiting unique physicochemical properties. The Scanning electron microscopy shows the different size and shape of particles oriented with rough surface. Using ImageJ software, the other distinguishing characteristics of surface morphology, and particle size analysis are performed. The elemental analysis demonstrates the cellulose's organic nature by demonstrating its higher carbon and oxygen content. On the basis of the physicochemical characteristics of the celluloses, it could be considered as alternative sources of cellulose for potential value-added industrial applications and more applicable for the polymer composite reinforcement filler material.

Keywords *Citrus x sinensis* peel · Fruit Waste · Cellulose · Waste utilisation · Biomass · Biofiller

✉ Murugesan Palaniappan
mpapathi@imamu.edu.sa

Sivasubramanian Palanisamy
sivaresearch948@gmail.com

¹ Department of Mechanical Engineering, College of Engineering, Imam Mohammad Ibn Saud Islamic University, Riyadh 11432, Kingdom of Saudi Arabia

² Department of Mechanical Engineering, P T R College of Engineering & Technology, Thanapandiyan Nagar, Austinpatti, Madurai-Tirumangalam Road, Madurai 625008, Tamilnadu, India

³ Department of Chemical Engineering, College of Engineering, Imam Mohammad Ibn Saud Islamic University, Riyadh 11432, Kingdom of Saudi Arabia

⁴ Department of Mechanical and Aerospace Engineering, Carleton University, 1125 Colonel By Drive, Ottawa, ON K1S 5B6, Canada

⁵ School of Science and Technology, University of Camerino, 62032 Camerino, Italy

Introduction

Materials derived from lignocellulosic materials have garnered a lot of attention in the green industry due to the fact that they are abundant, relatively inexpensive, and favourable to the environment. Agro-industries produce a substantial quantity of cellulosic waste; repurposing these cellulose-rich by-products can effectively tackle ecological and economic issues. The most abundant polysaccharide generated by bacteria and plants in nature is cellulose. Celluloses are predominantly derived from conventional sources, including wood and cotton. For many years, cellulose and its derivatives have been manufactured from these sources for a variety of industrial purposes, including the pharmaceutical, textile, and paper sectors. Too much use of natural resources makes problems like pollution, lack

of water, and bad waste management even worse around the world [1, 2]. Due to global resource scarcity, scientists will exert considerable effort to develop research methods that are less detrimental to the environment. This will also increase demand for products made from renewable materials. There are many places where across the globe, approaches integrating 'Waste to Prosperity' and 'Zero-Waste Initiative' have been comparatively heavily underscored as solutions to the aforementioned challenges [3, 4]. Among other nanotechnology-focused activities, material science research for the new development of bio composites is at the front of such activities in an effort to realise a sustainable society [5, 6]. For the sake of sustainable development, numerous researchers and scientists are being encouraged to recycle these types of garbage in order to lessen their harmful effects [7, 8]. These materials possess the capacity to be utilized in numerous value-added products once they have been appropriately treated or recycled, as opposed to being discarded or underutilized [9, 10]. The quantities and characteristics of microcrystalline cellulose are depending upon the extraction method, the place of origin, and the longevity of the natural substance. As a biopolymer, cellulose is very good at absorbing metals, synthetic colours, pesticides, carbon dioxide, and other organic and inorganic pollutants because it has reactive hydroxyl groups in its structure [11, 12]. In addition to crystalline and amorphous areas, cellulose is made up of a straight line of anhydro glucose monosaccharide units. 1,4- β linkages connect these parts to each other [13, 14]. It is very hard to get cellulose out of a plant cell wall that would be tightly wrapped inside the plant or from a different source. Mechanical and chemical processes are widely employed in the process of cellulose breakdown. Frequently, these sources consist of trace elements, cellulose, hemicellulose, lignin, and extractives. The curving-oriented cellulose serves as a reinforcing component within the cell walls, which are composed of a soft lignocelluloses and lignin matrix. Pure cellulose is produced through an efficient elimination procedure of hemicellulose, lignin, and other contaminants [15]. Environmental protection is promoted through the use of eco-friendly materials, which disintegrate rapidly in the environment [16]. As a result, the quantity of goods manufactured using renewable resources has increased significantly during the past several years. Different sources of cellulose have led to the creation of different types of cellulose particles, like micro-nano cellulose and fiber. A homopolymer of carbohydrates linked together with both amorphous and crystallised areas like lignin, polysaccharide, and cellulose. An estimated one-third of agro-industrial waste is composed of bio material, which is an extractive combination of hemicellulose and lignin [17]. Various techniques for chemical, mechanical, and biological isolation can induce alterations in the polymer's size and shape. So, different types of the polymer can

be separated, such as cellulose fiber, nanocrystals cellulose, microcrystalline cellulose, and microbial cellulose nanocrystals. Microcrystalline cellulose finds many applications in the paint and powder coating industry, cosmetics and toothpaste, food, welding electrodes, ceramics and sanitary ware, pill excipients, and textiles, among others, on account of its size and shape [18, 19]. As a reinforcing agent in composite materials, microcrystalline cellulose has gathered particular interest due to its potential advantages, which include insolubility in water, compatibility with materials, biodegradability, renewability, and a large surface area that promotes stronger resin bonds and optical transparency [20–22]. As a consequence of environmental consciousness and the circular economy, certain articles have included vegetable waste in its whole into starch matrices in an effort to enhance the qualities of starch composites. Orange peel (OP) is a particularly promising byproduct among whole vegetable discards, given that orange is the most plentiful fruit crop globally. Thousands of bio waste such as peels and other debris (pulp, seeds, damaged fruit, or fruit that does not satisfy quality standards) generated during the processing of citrus fruits and are typically classified as agro-industrial waste. Sweet oranges (*Citrus x sinensis*) comprise around 70% of the overall production and consumption of citrus fruits [23]. Annually, their processing generates around 16 million tonnes of waste, or approximately 30–40 percent of the fruit by weight. Sixty to sixty-five percent of this waste consists of peel, whereas thirty to thirty-five percent comprises pulp and seeds. Ignoring to treat these waste materials typically leads to their disposal without any practical repurposing, hence contributing substantially to environmental contamination. For this reason, the peel of the orange fruit is utilised in our research. The waste was enormously available and rich source of cellulosic material and easy to extract. Orange peel is formally referred to as *Citrus x sinensis* and is classified within the botanical family Rutaceae [24]. Monomers from cellulose are the simplest natural polymers to produce. Some researchers used pyrolysis, thermal pre-treatment, thermal decomposition, ammonia fibre detonation, carbon dioxide eruption, and other methods to treat lignocellulosic materials before they were used [25]. The cellulose content of the orange hybrid between pomelo (*Citrus maxima*) and mandarin (*Citrus reticulata*), and sweet oranges (*Citrus x sinensis*) that was isolated in this investigation through the utilisation of chemical processes including alkali treatment, acid treatment, and bleaching. To describe the extracted cellulose in this study, FT-IR spectroscopy, X-ray diffraction, scanning electron microscopy, atomic force microscopy, particle sizer analysis, and UV analysis were all used. The objective of this study was to investigate alternative cellulose sources from the aforementioned plant byproducts through characterization of their physicochemical properties for potential industrial applications with added value, using simple,

chlorine-free, and environmentally friendly extraction methods. The objective of this study was to investigate alternative cellulose sources from the aforementioned fruit byproducts through characterization of their physicochemical properties for potential industrial applications with added value, using simple, chlorine-free, and environmentally friendly extraction methods. As far as our knowledge extends, there are currently no reports pertaining to the extraction of MCC from biomass derived from orange peel fruit waste. The primary aim of this study is to isolate and analyse the MCC compound present in the peel of *Citrus x sinensis* (CSP).

Materials and method of extraction

Materials required

The orange peel was obtained from the oranges that were thrown after undergoing the juicing process by an adjacent restaurant in Tamil Nadu, India. Orange peel was crushed and oven-dried for four days at 50 °C. Suja Chemicals Nagercoil supplied the necessary chemicals, including hydrogen peroxide (bleaching), hydrochloric acid (for acid hydrolysis), and sodium hydroxide (for delignification).

Method of extraction

The extraction procedure of orange peel cellulose was illustrated in Fig. 1. The orange peel that was gathered was rinsed with water before being exposed to sunlight for a duration of 12 h in order to eliminate any residual moisture [26]. About 50 g of the de moisturized peel were placed in a 250 ml beaker and subjected to 6 h of heating

at the rate of 50 °C with 40% 1:5 (w/v) sodium hydroxide. After allowing the solution to cool, any surplus lignin or amylopectin was eliminated by filtering the liquor. Following filtration, the remaining bulk residue was acid hydrolysed with 50% 1:3 (v/v) hydrochloric acid that was extremely potent for 2 h. The solution containing non-cellulosic components were filtered and separated. Following this, the filtered residue obtained was washed with water to remove the acid content. The acquired mass was subsequently bleached with a mildly hazardous bleaching chemical known as 40% hydrogen peroxide [27]. The final product, cellulose with a white kind, was then dried in an oven preheated to 60 °C for an hour after a thorough rinsing with water. After being powdered with a ball mill, the dried cellulose was thereafter placed in a desiccator to avoid impurity and moisture contractions.

Characterization of cellulose

FT-IR analysis

In order to do FTIR analysis, the measurements were executed using a Nicolet 6700 spectrometer in wavelength region, with a fine resolution 4 cm⁻¹. The spectrometer has a range of 500 to 4000 cm⁻¹, at a resolution of 4 cm⁻¹. FTIR spectra were obtained following the process of pelletizing with KBr so as to illuminate the modifications that took place in the functional groups [28, 29]. The vibrational peaks observed in the ensuing spectra are attributable to the stretching of various chemical bonds associated with particular functional groups.

Fig. 1 Extraction of cellulose from *Citrus x sinensis* peel cellulose



Physical and chemical analysis

It was possible to figure out the density, weight reduction %, and yield proportion of the cellulose samples [30]. The following formula was used to sort out the weight loss percent for the chemically processed CSPC:

$$\text{Weight loss \%} = \frac{X_1 - X_2}{X_2} \times 100 \quad (1)$$

where X_1 = initial weight of orange peel and X_2 = The ultimate mass of the treated CSPC generated subsequent to the finish line of all phases. Additionally, the cellulose percentage of the CSPC that was separated following chemical treatment was documented as a crucial organic property. The percentage of yield was computed utilising the below equation:

$$\text{Yield \%} = \frac{W_2}{W_1} \times 100 \quad (2)$$

where W_2 and W_1 are the weight of CSP cellulose and weight of orange peel respectively [31].

X-Ray diffraction analysis

A study was undertaken to ascertain the degree of crystallinity shown by cellulose by the utilisation of X-ray diffraction (XRD). This analysis was carried out with a PW3040/60 X'Pert analyser (United Kingdom) with $\text{Cu-K}\alpha$ radiation ($\lambda = 0.154056 \text{ nm}$). The current passing through the filament was 30 mA, while the voltage at which it operated was 40 kV. Using a step size of 0.02° , the samples were tested in the interval of 5° to 30° of 2θ [32]. In the subsequent step, the crystallinity index was determined by employing the origin pro software. In a similar manner, the measurement of crystallite size was carried out by means of Scherrer's Eq. (4), wherein the symbol CS represents the size of the crystallite in nanometres, K represents Scherrer's constant, which is 0.89, λ and β represent the wavelength and full-width at half-maximum of peak, and θ represents Bragg's inclination ($^\circ$). The crystalline peak area value that was received from the Origin Pro 2021 programme was utilised in the calculation of the crystallinity index of the sample [33].

$$\text{Crystallinity index \%} = \frac{\text{crystalline peak}}{\text{crystalline peak} + \text{amorphous area}} \times 100 \quad (3)$$

The average crystallite size (nm) in the plane perpendicular to the lattice plane was calculated utilising the Scherrer equation.

$$\text{Crystalline size (CS)} = \frac{k\lambda}{\beta \cos\theta} \quad (4)$$

Surface morphology, elemental analysis, and particle size analysis

The CSPC scanning electron microscopy (SEM) and energy dispersive x-rays (EDX) procedures were executed utilising a Hitachi S-3400N SEM that had EDX capabilities. An accelerating voltage of 15 kV was utilised for either procedure. Before the specimen was analysed, the sputtering gold coating was applied to it in place to avert charging from occurring [34]. The exterior properties as roughness/smoothness, existence of voids, and other unwanted particles were examined to illuminate the adhesion and interfacial bonding property of the CSP MCC. EDX analysis, which was carried out at a magnification of one thousand times, was utilised in order to ascertain the element composition of the samples. The determination of the size of particles of CSP cellulose was eventually accomplished by the usage of the ImageJ software [35].

Thermal analysis

Using a TGA (Diamond TGA/DTA Perkin Elmer) instrument, the measurement of the cellulose sample was performed at a heating rate of $10^\circ\text{C}/\text{min}$ under a nitrogen atmosphere (20 ml/min) [36]. After obtaining a sample weight of 9.833 mg, the sample was stored in a desiccator until it was weighed. The cellulose sample was subjected to TGA analysis in order to study the characteristics of degradation that were present in the sample. First, the sample was maintained at a temperature of 40°C . It was then heated at a rate of ten degrees Celsius per minute, with temperatures ranging from four hundred to one thousand degrees Celsius. In order to obtain a more precise temperature data from the thermostat and to gain an even more precise result from the thermocouple, a progressive heating rate was chosen as the method of heating [37].

UV analysis

The UV-vis analyzer (V-530, Jasco, Japan) data was utilised in order to ascertain the UV absorption patterns of the cellulose. The experiment was carried out with temperatures ranging from 30 to 320 degrees Celsius, 350 watts of electricity, and an amplitude of 60 Hz. For the purpose of powering the machine, a frequency of 20,000 Hz was utilised. In order to produce a liquid sample, two grammes of CSPC are dissolved in a suitable solvent at a weight-to-volume ratio of 1:3. The components that have not yet dissolved are filtered, and the liquid that is produced as a result is placed in the sample container so that the values can be measured [38].

Atomic force microscopic analysis

The surface adhesion properties were assessed using scanning electron microscopy (SEM); yet, atomic force microscopy provides more accurate findings, especially in the absence of topographical investigation (AFM). In the course of this research, high-resolution observations were carried out in 2D and 3D at a granularity of 0.1 nm utilising a Park XE-100 atomic force microscope [39]. This study identified the important roughness characteristics, including the root mean square roughness (R_{rms}), average surface roughness (R_a), roughness skewness (R_{sk}), and roughness kurtosis (R_{ku}), as well as the 10-point average surface roughness (R_z) and maximum peak-to-valley height (R_t).

Result and discussion

FT-IR spectroscopy analysis

A presentation of the findings obtained from the Fourier transform spectroscopy can be described in Fig. 2. On the basis of the results, the functional groups contained in CSP cellulose may be identified. The band that may be found at 3332.09 cm^{-1} is caused by the presence of OH stretching [40]. In order to determine whether or not phenols, alcohols, and polysaccharides are present, hydroxyl groups might be utilised as a stand-in for these substances. C-H stretching is responsible for the tiny peak that can be found at 2892.34 cm^{-1} [41]. The weak band observed at a wavenumber of 2892.34 cm^{-1} can be ascribed to the asymmetric stretching vibration of CH present in lignin, hemicellulose, and every glucose unit of cellulose. At a frequency of 1618.35 cm^{-1} , a significant peak is produced

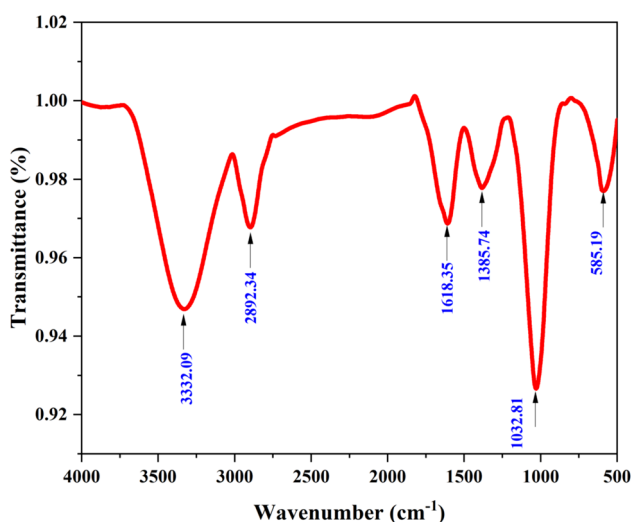


Fig. 2 FT-IR analysis of CSP cellulose

by the C=C vibrations of alkenes. In the frequency range of 1029.69 cm^{-1} , the high and abrupt peak is the result of C–O–C stretching [38]. The stretching frequency of the CH_2 group is responsible for the peak that can be found at 1385.74 cm^{-1} . Additionally, this is a result of the CH and C–O groups of the pyranose ring in cellulose undergoing in-plane bending vibrations. The absorbance bands at 1032.81 cm^{-1} and 3332.09 cm^{-1} are attributable, respectively, to the C–O–C stretching brought about by the pyranose ring and the O–H straining brought about by the hydroxyl groups [42]. The elongation of cellulose signifies the presence of a pyranose ring and C–O–C bonds, which contribute to its structural integrity [43]. The observed increase in peak intensity at 1032.81 cm^{-1} indicates that the chemical treatments have led to a corresponding rise in the cellulose content of the material. The structure of cellulose can be understood through the utilisation of these functional characteristics. It was not possible to identify the functional groups of hemicellulose (esteric) and lignin (C=O) in the CSP cellulose examination results. The result of the chemical separation was cellulose in its purest form. Different studies also reported similar findings, demonstrating that non-cellulosic components might be removed under various treatment conditions.

Physical and chemical analysis

CSP cellulose obtained from the plant byproducts was odourless and white in appearance. A density of 1.413 g/cm^3 was discovered for the CSP cellulose. According to the results of the calculation using Eq. (1), the cellulose yield is 67.82%. Then, there is responsible weight loss occur due to the elimination of lignin (12.8%), wax, and minerals (4.2%), and bleaching process residue(13.5%) [44]. A tabular representation of the yield percentage and density of microcrystalline cellulose can be seen in Table 1. According to the table, the literature on cellulose recovered from tea trash only produced 30.54% cellulose, and the density was found to be 1.324 g/cm^3 [45]. The yield percentage in our study is notably high in comparison to other resources, including cotton (80.08%), banana peel cellulose (59.18%), *borrasus flabellifer* flower cellulose (59.1%), and pineapple leaf (70.9%) [46]. The use of such a high proportion of waste material is mostly for application purposes. The chemdraw programme was employed to depict the cellulose structure, which is seen in Fig. 3. The structure exhibits the presence of 1,4 β - glucopyranose links and an excessive number of OH groups.

X-ray diffraction analysis

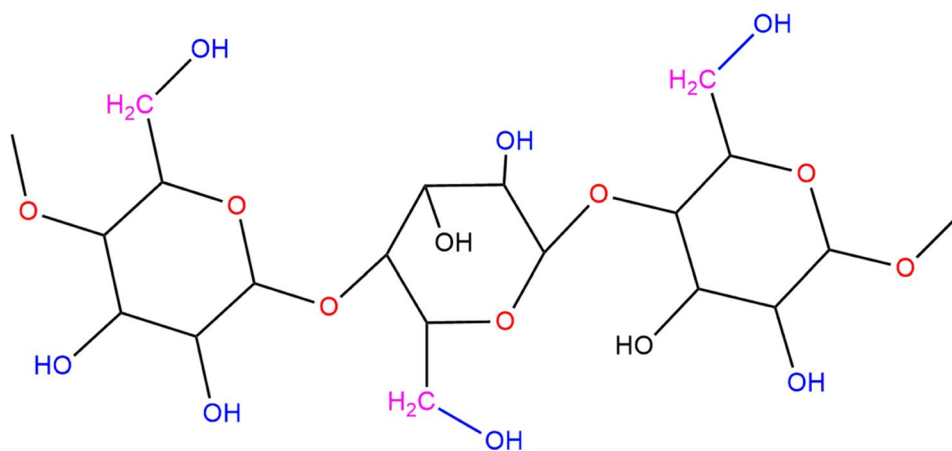
Figure 4 depicts the outcomes derived from the X-ray analysis results of the CSP cellulose sample. The process of cellulose crystallisation is promoted by intramolecular hydrogen

Table 1 Density and yield % of cellulose samples from various sources

Sl. No.	Sources	Yield (wt.%)	Density (g/cm ³)	Cellulose (%)	Reference
	Sugarcane bagasse	39.05	-	77.16	[47]
	<i>Borassus flabellifer</i> flower flower	59%	0.36	73.2	[48]
	TSMCC	44.15	1.561	90.57	[49]
	<i>Azadirachta indica</i> A. Juss	68.73 ± 1.13	1.59	96.53	[50]
	<i>Saccharum spontaneum</i>	83	-	83.33 ± 0.47	[51]
	Date palm seeds	-	-	97.3	[52]
	Coffee hull	35.05	-	79.9 ± 0.46	[34]
	Soybean hulls	-	-	83.78 ± 1.90	[53]
	Pineapple leaf	70.9–81	-	85.53 ± 2.3	[54]
	Millet	65–70	-	85.2 ± 1.9	[55]
	Peanut oil cake	-	1.58	82.3	[56]
	Rice straw	66.2–64.7	-	71.2	[57]
	Rice husks	86	-	91.92	[58]
	Walnut shell	35.36 ± 1.14	-	79.24 ± 2.51	[59]
	Napier grass	52	-	93.5	[60]
	Ficus leaf	55	-	90.6	[61]
	Corn cob	27.24 ± 2.63	-	83.13 ± 2.63	[62]
	<i>Citrus x sinensis</i>	67.82	1.413	70	This study

bonds maintained in place by a weak Vander Waals force [63]. Variable-intensity diffractograms were discernible within the angles $2\theta = 15^\circ - 30^\circ$. A significant number of ranges characterised by intense peaks also possess a high crystallinity index. Crystallinity of the sample was determined by the crystalline peaks at 15.01 and 22.06, which corresponded to lattice planes of 1 1 0 and 2 0 0, respectively [64]. In the interplane space of the cellulose lattice is the amorphous area [65]. Numerous investigations have established that the majority of cellulose materials exhibit a simple three crystalline peaks. The determination of the crystallinity index of the cellulose is accomplished by the peak

technique. The origin programme was utilised to record the overall area and the area of crystalline peaks [66]. Equation (3) was employed to determine the crystallinity index, which yielded a value of 72.54%. The crystalline size of 9.63 nm was calculated using Eq. (4). Table 2 presents the crystallinity index of a selection of cellulose materials. Compared to other celluloses, corn cob cellulose has a lower crystallinity index (49.58%), as indicated in the table of literature [67]. The crystallinity index of the cellulose extracted from brown algae (74.23%), sugarcane baggase (70.64%), olive fibre (74.2%), *manau rattan* (72.42%), *saccharum spontaneum* (74.06%), and alfa fibre (73.63%) is average with the

Fig. 3 Chemical structure of CSP cellulose**Citrus x sinensis peel cellulose chemical structure**

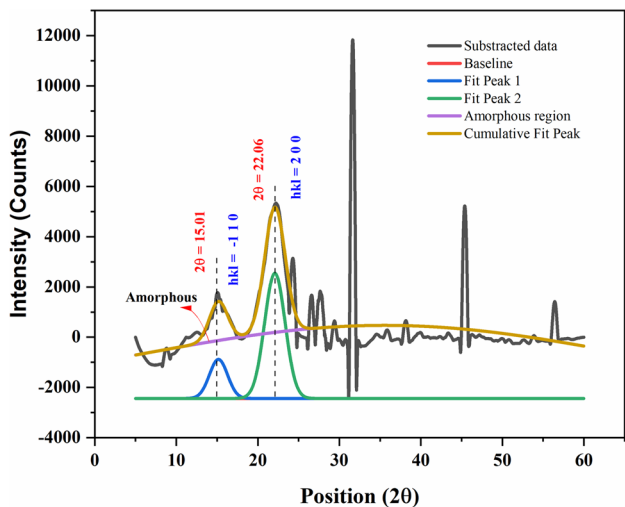


Fig. 4 X-Ray diffraction analysis of CSP cellulose

cellulose extracted from orange peel. The crystallinity index is high for the tea waste (81%), rice straw (82.4%), waste cotton fabrics (85.32%), and fodder grass (80%). The higher crystallinity index may be due to the type of acid used for the microcrystalline cellulose extraction process. In a literature of waste cotton fabric, the acid utilised is nitric acid and hence the crystallinity is higher than others that are extracted using mild acids such as hydrochloric acid and acetic acid. In our study hydrochloric acid is used however, the crystallinity

Table 2 Crystallinity index and crystallite size comparison with other sources

Sl. No	Source of MCC	Crystallinity index (%)	Crystallite size (nm)	Reference
1.	Brown algae	74.23	-	[68]
2.	Sugarcane bagasse	70.64	4.42	[47]
3.	Waste cotton fabrics	85.32	4.65	[69]
4.	<i>Borassus flabellifer</i> flower	69.81	44.28	[48]
5.	Soybean hull	70	-	[70]
6.	Neem oil cake	70	-	[71]
7.	<i>Saccharum spontaneum</i>	74.06	-	[51]
8.	Tea waste	81	2.09	[72]
9.	Commercial MCC	74–80.60	-	[73]
10.	Alfa fiber	73.62	3.68	[74]
11.	Rice straw	82.4	3.97	[57]
12.	Corn cob	49.58	210.36	[62]
13.	<i>Manau rattan</i>	72.42	-	[75]
14.	Olive fiber	74.2	-	[76]
15.	Fodder grass	80	2.45	[77]
16.	<i>Citrus x sinensis</i>	72.54	9.63	This study

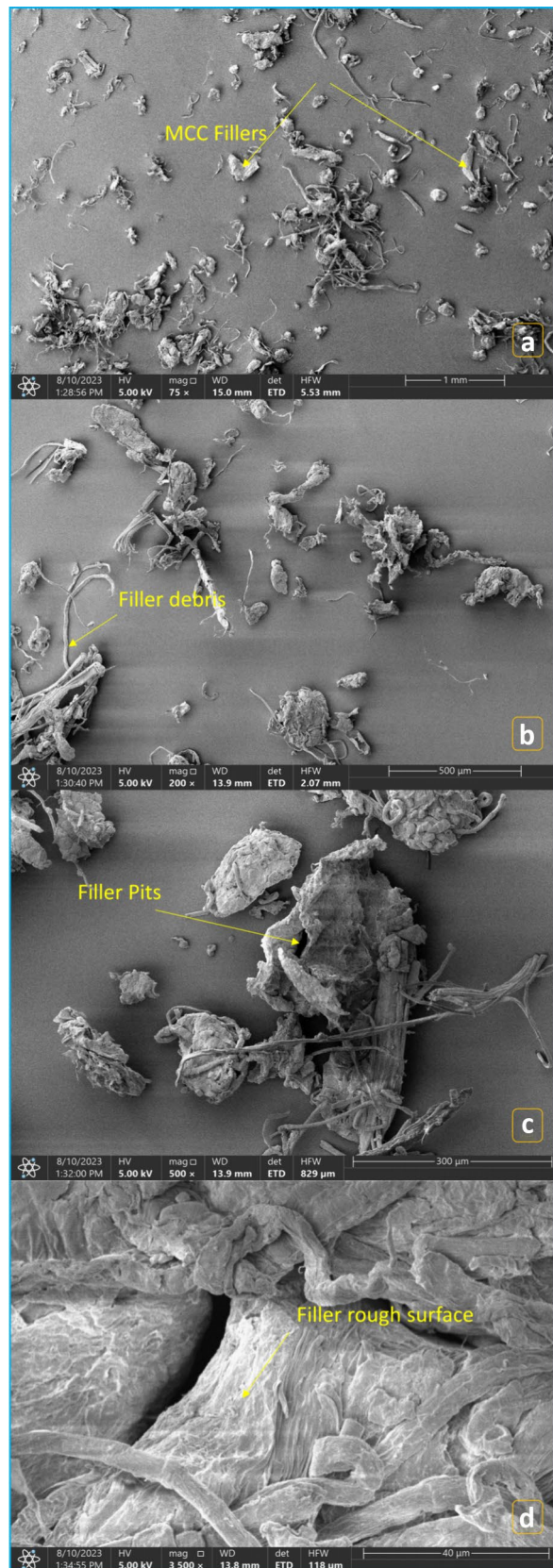


Fig. 5 Scanning electron microscopy analysis of CSP cellulose

index is similar to the most of the cellulose resources shown in the Table 2. The relationship between crystalline size and crystallinity index is inversely proportional; as the crystallinity index rises, crystalline size decreases progressively. During the chemical treatment, some crystalline components may be introduced, which raises the crystallinity index but reduces the crystalline size.

SEM analysis

The investigation includes SEM graphs of the cellulose sample extracted from the peel of *Citrus x sinensis*. Typically, natural plant fibres are composed of a number of overlapping elementary fibres (also known as ultimate fibres or cells) that are securely held together along their length by pectin and other non-cellulosic substances that provide the bundle with its overall strength. As seen in Fig. 5(a), the acid degraded bleached cellulose-containing fiber-like substance possesses a rod-shaped morphology. The chemical treatments that were implemented enabled the elimination of surface contaminants and non-cellulosic fractions that were found in the CSPC. Alongside its minuscule spherical morphology, cellulose exhibits a rough exoskeleton, as seen in Fig. 5(b). The photographs presented are comparable in nature to the cellulose that is extracted from the fine pith core of cotton stalks [78]. Numerous filaments of cellulosic microfibrils were identified in Fig. 5(c) and (d). Figure 5(c) illustrates how the concentration and clearance of metallic particles resulted in the formation of the pits. A chemical process has produced the filler debris's abrasive surface. Several investigations have

documented the elimination of non-cellulosic and cementitious substances, including wax, lignin, and hemicelluloses, while extracting isolated microcrystalline cellulose from lignocellulosic materials using various chemicals. It was determined that the lowest and maximum lengths of the extracted celluloses were considerably reduced (0.066 and 0.408 μm , respectively), with an average length of 0.137 μm . These results suggest that the treatment conditions effectively eliminated non-cellulosic components.

TGA analysis

The thermal degradation characteristics of CSPC are represented in Fig. 6 via TGA curves. The mass of CSPC remains constant at temperatures below 50 $^{\circ}\text{C}$. With a determined mass change of 0.52 mg, the early phase degradation commences at temperatures surpassing 50 $^{\circ}\text{C}$ and persists until 150 $^{\circ}\text{C}$. In this process, the moisture and volatile compounds included in the cellulose are removed [79]. The degradation is particularly severe during the second period. During this phase (200–350 $^{\circ}\text{C}$), a mass change of 2.770 mg was detected. During this phase, significant cellulose components may undergo disintegration of smaller molecules and opening of the pyranose ring. Sugarcane bagasse MCC lost 75% of its weight from 263 to 378 $^{\circ}\text{C}$ while NCCF lost 68% at 150–568 $^{\circ}\text{C}$ [80]. A marginal alteration in mass is observed solely above 450 $^{\circ}\text{C}$, which signifies that lignin has been entirely removed through chemical treatment. The ultimate deterioration process persists until 800 $^{\circ}\text{C}$, yielding a mere 3.70 mg of remaining mass [81]. The highest

Fig. 6 TGA analysis of CSP cellulose

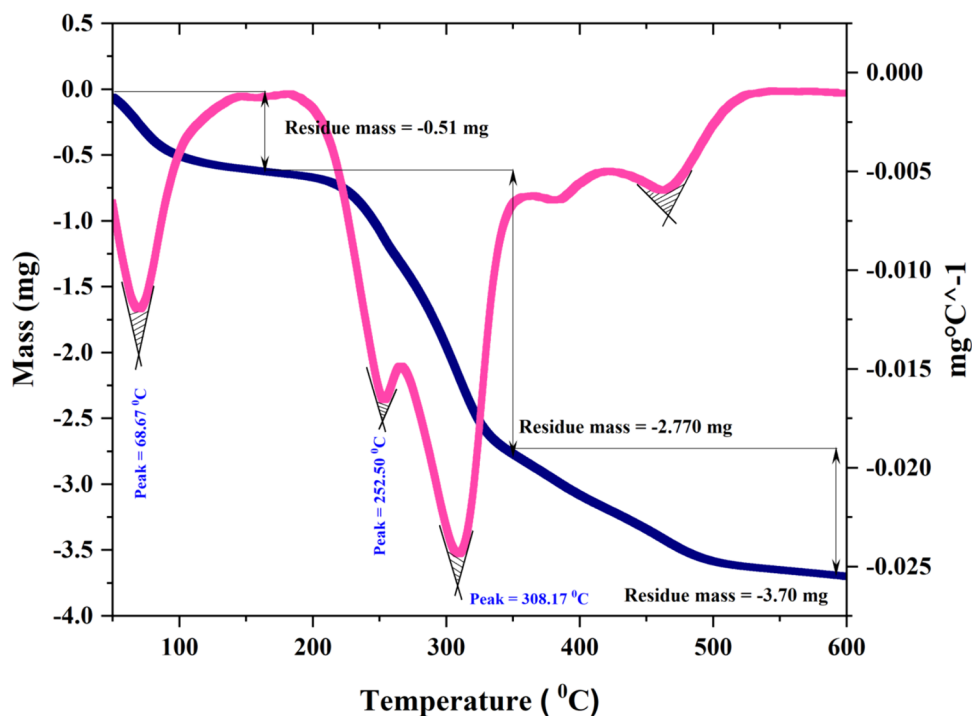


Table 3 Thermal degradation behaviour of some cellulose from various sources

Sl. No	Source of MCC	Thermal resistance (°C)	Reference
1.	Commercial MCC	220–300	[24]
2.	Oil palm biomass	250	[83]
3.	Neem oil cake	300	[71]
4.	<i>Borassus flabellifer</i> flower	208	[84]
5.	Soybean hull	250	[70]
6.	Waste cotton fabrics	250	[69]
7.	Brown algae	302.69	[85]
8.	Tamarind seed MCC	230	[86]
9.	<i>Saccharum spontaneum</i>	338	[51]
10. A	Sugarcane bagasse	264.15	[87]
11.	Cotton stalk	289.7	[83]
12.	Fodder grass	286	[77]
13.	Tea waste	230	[88]
14.	Olive fiber	286.1	[39]
15.	Walnut shell	260.96	[38]
16.	<i>Citrus x sinensis</i>	308.17	This study

breakdown temperature of cellulose is detailed in Table 3. In comparison to the other types of cellulose shown in the table, the breakdown temperature of CSP cellulose is higher. The resources such as neem oil cake (300 °C), brown algae (302.69 °C), *saccharum spontaneum* (338 °C) are having highest withstanding temperature that is above 300 °C. The remaining cellulosic resources listed in the table are showing lower degradation temperature below 280 °C. The cellulose with higher withstanding temperature is preferable for the

polymer composite reinforcement applications. Three phase shifts are shown in the DTA curve analysis, and each deterioration temperature is roughly equivalent to the analytical data from the TGA. The deterioration cellulose moiety is responsible for a little phase shift peak at 252.50 °C. The breakdown of the cellulose molecule into smaller parts is the cause of the substantial rate of degradation at 308.17 °C, which is also the highest temperature at which CSP cellulose degrades [82].

EDX analysis

The energy-dispersive analytical results accumulate in Fig. 7. Primary components of the organic compound cellulose are carbon, hydrogen, and oxygen. Elements may undergo modifications as a result of the chemical treatment. The atoms carbon and oxygen have the highest abundances in the dataset, accounting for 35.5% and 42.6% by wt.%, respectively. The insignificance of the existence of additional elements, including nitrogen (4.8%), sodium (3.4%), chlorine (3.1%), and silicon (10.45%), is attributed to impurities introduced by chemical processes including alkali treatment, solvent treatment, and slow pyrolysis [89]. Other studies also reported the presence of organic compounds in the cellulose extraction process.

Particle size analysis

Using ImageJ software, the size of the cellulose particle is found out from SEM pictures. Each particles have different size and shape which is explicit in SEM image. About

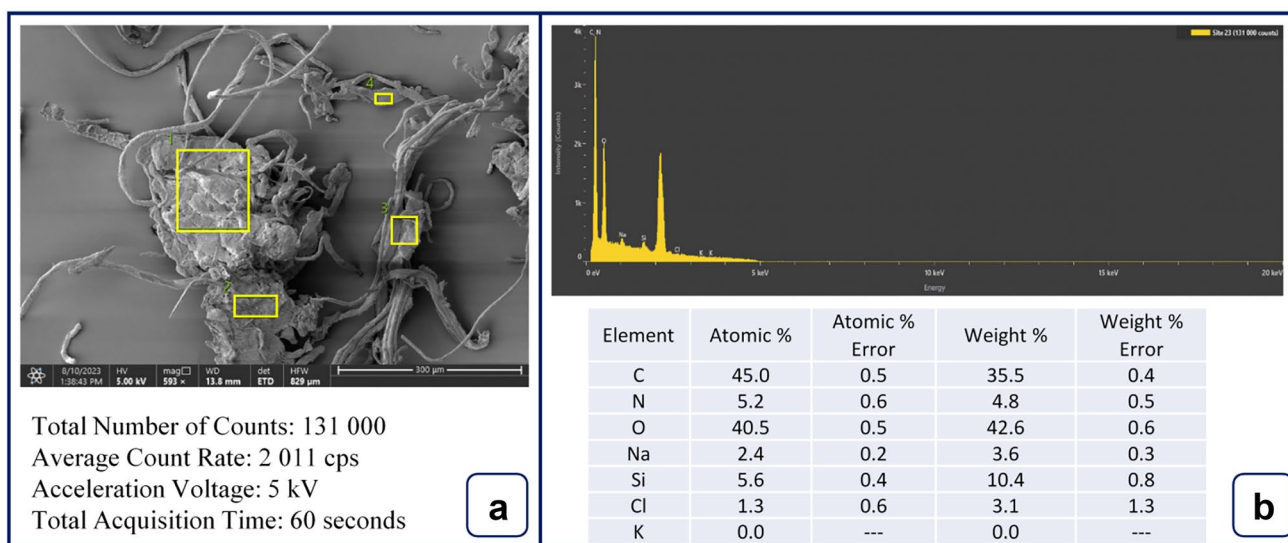
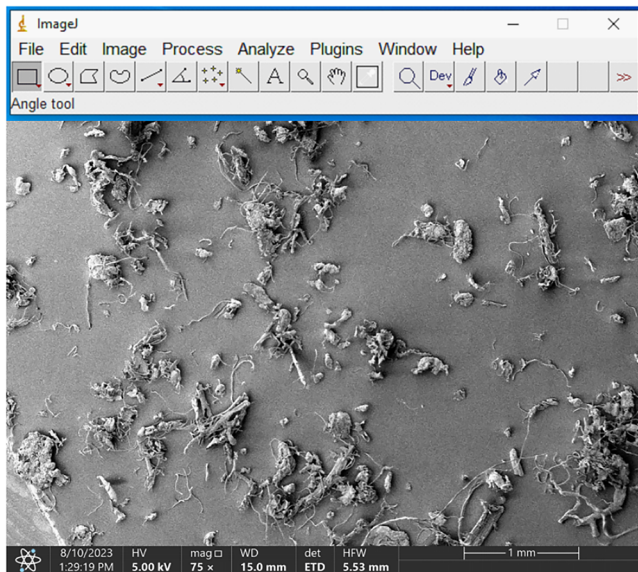


Fig. 7 EDX analysis of CSP cellulose

25 places are selected and measured the length, mean and standard deviation data using ImageJ software. The software read the size of the particle at each phase with different numerals. The average of 25 particles gives the proper particle size of the CSP cellulose. The histogram was plotted using the data obtained from 25 places and standard deviation of the particles also found. The findings of ImageJ, the data, the threshold image, and the histogram are illustrated in Fig. 8(a)–(d), respectively. The particle counts are

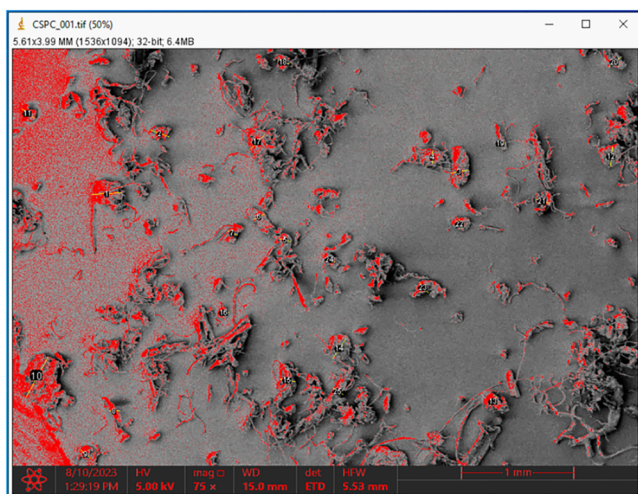
utilised to determine their micrometre size. Greater quantities of 0.05–0.15 μm -sized particles are detected in 25 of the samples. The remaining particles have dimensions of 0.40–0.45 μm (1 counts) and 0.15–0.20 μm (4 counts). The particle has a mean size of 0.137 μm , with a corresponding standard deviation of 0.072. Particle size is entirely determined by the physical and chemical treatments of cellulose [90]. There exists variation in the orientations of particles across different locations. Agglomerate particles



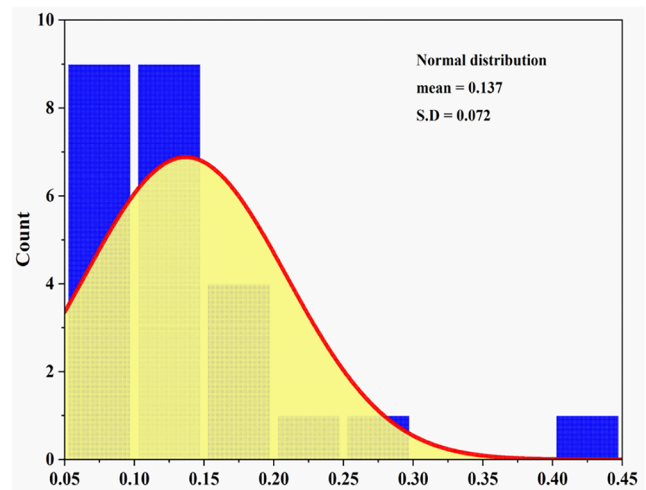
a

Label	Area	Mean	Std.Dev	Min	Max	Angle	Length	
1	9.72E-04	183.784	41.763	80.667	254	3.18	0.263	
2	6.39E-04	165.232	53.72	40.099	243.01	-19.983	0.171	
3	5.86E-04	136.219	33.225	54.445	204.255	10.784	0.156	
4	4.13E-04	145.065	33.593	84	212	-90	0.109	
5	3.73E-04	143.319	44.998	63.037	203.897	-12.995	0.097	
6	4.13E-04	150.447	26.016	58	207	-151.699	0.108	
7	3.33E-04	144.744	45.753	79.167	219.25	-24.444	0.088	
8	3.60E-04	170.778	59.348	76	253	0	0.095	
9	4.26E-04	168.309	52.174	40.866	247.919	-39.806	0.114	
10	0.002	154.822	50.287	7.357	240.531	-118.856	0.408	
11	5.06E-04	200.717	32.219	147.436	254	-36.254	0.136	
12	6.26E-04	118.741	33.02	37.87	207.913	-94.97	0.169	
13	3.60E-04	158.45	24.377	104.083	195.822	51.34	0.093	
14	7.86E-04	115.068	24.875	67.633	185	56.31	0.211	
15	4.93E-04	122.995	43.672	43	206	-9.462	0.133	
16	3.33E-04	159.68	52.815	78	254	0	0.088	
17	6.53E-04	180.806	26.96	115.833	234	45	0.175	
18	3.46E-04	126.289	54.581	12	212.851	-18.435	0.092	
19	2.53E-04	160.047	44.668	102.111	250	6.34	0.066	
20	5.19E-04	122.335	34.338	27	199	-141.34	0.14	
21	4.40E-04	148.958	61.823	38.078	249.27	-18.435	0.115	
22	2.93E-04	122.707	50.133	22.694	211	-73.301	0.076	
23	4.66E-04	150.52	76.035	5.716	241.135	-49.764	0.124	
24	3.33E-04	203.141	22.1	170.75	249.625	-24.444	0.088	
25	4.00E-04	134.855	75.027	1.36E-12	230.083	-33.69	0.105	
26	Mean	5.13E-04	151.521	43.901	62.234	226.582	-31.397	0.137
27	SD	2.65E-04	24.353	15.001	43.203	22.406	54.774	0.072
28	Min	2.53E-04	115.068	22.1	1.36E-12	185	-151.699	0.066
29	Max	0.002	203.141	76.035	170.75	254	56.31	0.408

b



c



d

Fig. 8 Particle size analysis of CSP cellulose

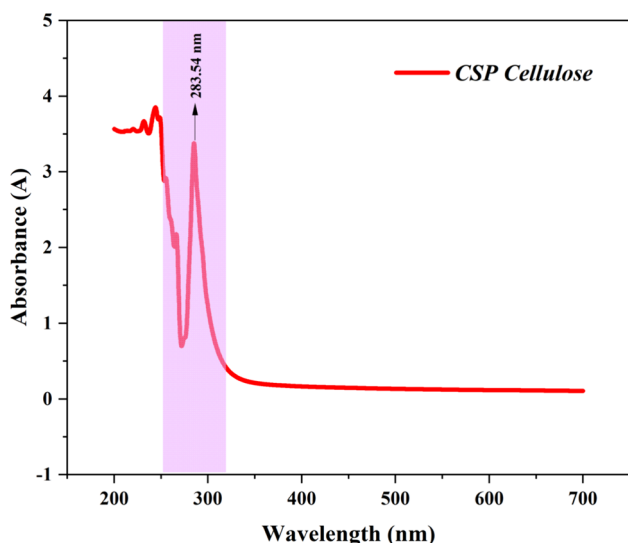


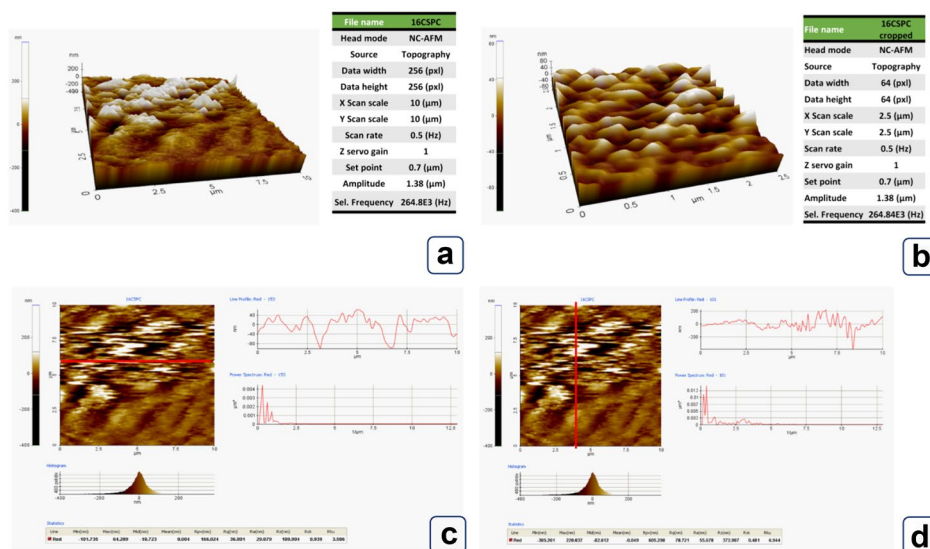
Fig. 9 UV analysis of CSP cellulose

are identified in specific geographical areas, characterised by their larger particle size compared to freely available particles [91]. Their length is evidently not significantly greater than their respective diameters. We anticipate that, in addition to functioning as filtering medium and sorbents, the CSPC will be useful for the production of regenerated cellulose films utilising water as the coagulant and an ionic liquid as the solvent.

UV analysis

The Fig. 9 depicts the ultraviolet–visible spectroscopy investigation of CSPC. The cellulose incorporates UV active functionals that demonstrate absorption at 283.54 nm [92]. The region of investigation was identified using a pink shading. The complete determinant of

Fig. 10 Atomic force microscopic analysis of CSP cellulose



ROUGHNESS PARAMETER	VALUE
Min (nm)	-101.735
Max (nm)	64.289
Mid (nm)	-18.723
Mean (nm)	0.004
R _{pv} (nm)	166.024
R _q (nm)	36.801
R _s (nm)	29.079
R _z (nm)	109.904
R _{sk}	0.938
R _{ku}	3.506

ROUGHNESS PARAMETER	VALUE
Min (nm)	-385.261
Max (nm)	220.037
Mid (nm)	-82.612
Mean (nm)	-0.049
R _{pv} (nm)	605.298
R _q (nm)	78.721
R _s (nm)	55.678
R _z (nm)	372.987
R _{sk}	0.481
R _{ku}	6.944

cellulose transparency is its crystalline structure. A cellulose material with a higher crystallinity index exhibits the ability to absorb an excessive quantity of UV radiation [93]. The UV absorption capabilities of cellulose render it a viable candidate for implementation as a bio composite reinforcement [94]. There is potential for the UV barrier properties of the cellulose filler to augment the barrier properties of the biofilm material.

AFM analysis

Conducting a surface roughness analysis on a 6×6 square centimetre region, as depicted in Fig. 10. Skewness, maximum length, minimum size, and mean size, kurtosis, average surface roughness, root mean square surface roughness, and ten-point average surface roughness are parameters of surface roughness that are tabulated in two separate ways: one for horizontal surfaces and one for vertical surfaces [95]. When the split is done vertically, the roughness skew value is higher than when it is done horizontally. In the horizontal direction, the average surface value ($R_a = 29.079$ nm) is lower than vertical direction ($R_a = 55.578$ nm). These statistics vary according to the geographical area under investigation [96]. Significantly influencing the morphology surface dimension of the final product are the chemical circumstances and variables under which cellulose are produced. The profile of

roughness measurement is illustrated in Fig. 10(c) and (d). The optical technique is utilised to ascertain the average particle roughness of the cellulose. The surface of a CSPC particle exhibited the least variation in roughness. The horizontal position has a considerably smoother surface than the vertical position. Additionally, the root mean square surface roughness ($R_q = 36.801$ nm, 78.721 nm), peak valley height surface roughness ($R_{pv} = 166.024, 605.298$) and 10-point average surface roughness ($R_z = 109.904$ nm, 372.97 nm) are other suitable surface roughness values of the cellulose. The values of kurtosis, skewness, highest, lowest, mid, and mean roughness are illustrated in Fig. 6, as an illustration (e & f). The feasibility of defining the CSPC particle with additional properties, including skewness and kurtosis, was investigated. Skewness (0.938, 0.481) is greater than zero for both horizontal and vertical direction due to the absence of fractures [97]. A positive value of kurtosis (3.506, 6.944) signifies that the surface has an average peak and possesses a good surface.

Roughness analysis

The surface roughness of CSP cellulose was resulted in the Fig. 11. The thresholding of sem image and the graphical representation is shown in Fig. 11(a) and (b). The surface activity and the parameters such as skewness, kurtosis, area

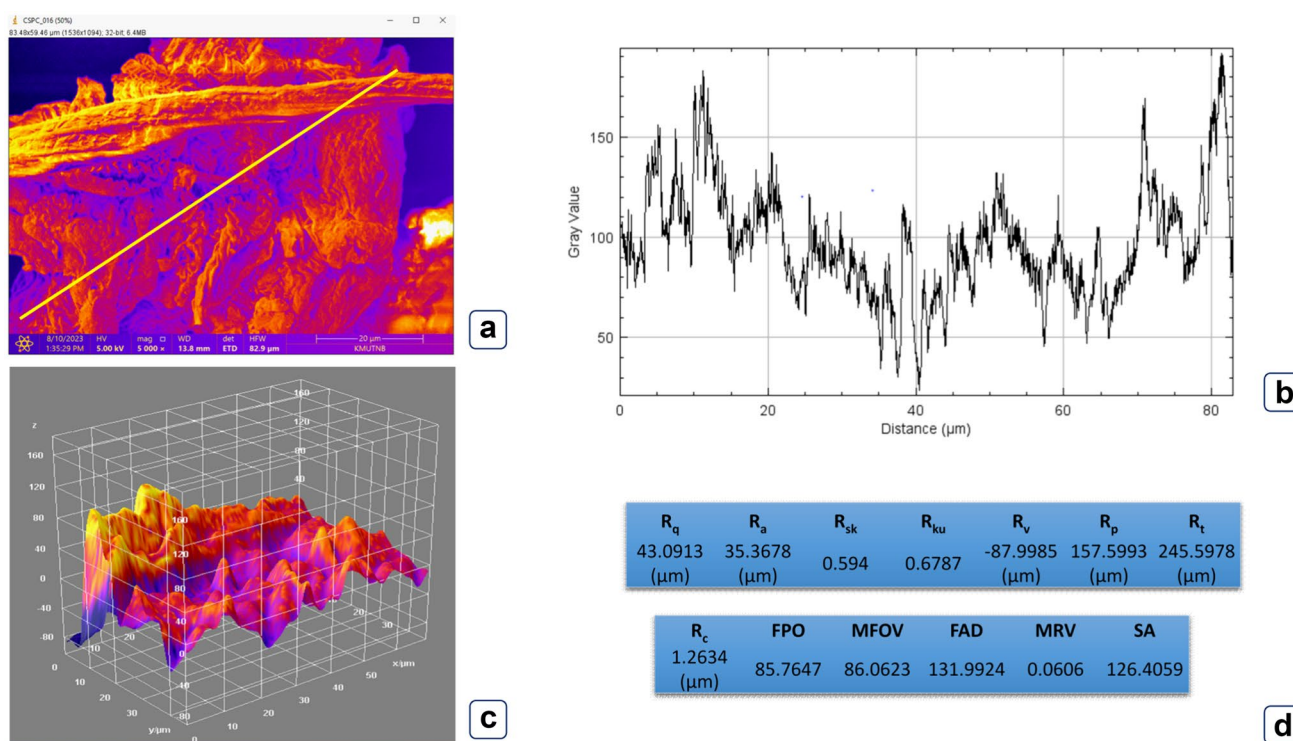


Fig. 11 Surface roughness of CSP cellulose

of surface roughness, vertical surface roughness and ten point average surface roughness are tabulated in Fig. 11(d). The average surface roughness of the cellulose is found to be $R_a = 35.3678 \mu\text{m}$. The skewness value ($R_{sk} = 0.594$) is less than three and the surface is minimally peaked [98]. The positive kurtosis ($R_{ku} = 0.6787$) show there is minimum surface break present. The CSP particles are had higher tenpoint average surface roughness ($R_t = 245.5978 \mu\text{m}$). On seeing every section of particle the average, maximum, minimum surface roughness is unique and there is no surface tension present in the particles with various size [99]. The surface of cellulose is allowable and smooth, fracture less surface is visible. Thus, the chemical treatments was not affect the surface of CSP cellulose. In addition, the authors want to increase the utility of CSPC as a raw material for cellulose films.

Conclusions

The cellulose was isolated ecofriendly from citrus and characterized the useful parameters. In this study, food waste material is optimally utilised and cellulose is extracted from *citrus x sinensis* peels through the excellent application of chemical procedures such alkalization, acid hydrolysis, and bleaching. The functional characteristics of extracted cellulose, such as surface form, density, particle size, transparency, and crystallinity, have been extensively studied. FT-IR was utilised by researchers to identify cellulose glycosidic connections and examine the arrangement of the structure. The density of cellulose is found to be 1.413 g/cm^3 and the yield % is noted as 67.82%. Scanning electron microscopy images show an abrasive structure that look like a cylinder shape. The crystallite size and crystallinity index were found to be 9.63 nm and 72.54%, respectively, using X-ray diffraction examination. The maximum rate of decomposition for the isolated cellulose, according to the thermal investigation using DTG curves, is $308.17 \text{ }^\circ\text{C}$. When the particle sizes were examined with ImageJ software, most of them had diameters less than $100 \mu\text{m}$. The cellulose that was removed might be more beneficial in the polymer composite filler reinforcement application. It's clear from the above that the byproducts may be valuable sources of cellulose for a variety of high-value industrial uses.

Acknowledgements The authors extend their appreciation to the Deanship of Scientific Research at Imam Mohammad Ibn Saud Islamic University (IMSIU), Saudi Arabia, for supporting and funding this research work through Grand No. IMSIU-RG23050.

Author's contribution Murugesan Palaniappan and Srinivas Tadepalli: Conducted all the experimental works and written original manuscript. All other Authors: Supported for data analysis and review the final draft.

Funding The authors extend their appreciation to the Deanship of Scientific Research at Imam Mohammad Ibn Saud Islamic University (IMSIU), Saudi Arabia, for supporting and funding this research work through Grand No. IMSIU-RG23050.

Data availability The data that support the findings of this study are available on request from the corresponding author. The data are not publicly available due to privacy or ethical restrictions.

Declarations

Ethical approval Not applicable.

Consent to participate Not applicable.

Consent to publish Not applicable.

Competing interests The authors declare that they have no known competing financial interests or personal relationships that could have appeared to influence the work reported in this paper.

References

- Divya D, Suyambulingam I, Sanjay MR, Siengchin S (2022) Suitability examination of novel cellulosic plant fiber from *Furcraea selloa* K. Koch peduncle for a potential polymeric composite reinforcement. *Polym Compos* 43:4223–4243. <https://doi.org/10.1002/PC.26683>
- Giacon VM, Rebelo VSM, dos Santos GM et al (2021) Influence of mercerization on the physical and mechanical properties of polymeric composites reinforced with amazonian fiber. *Fibers and Polymers* 22:1950–1956. <https://doi.org/10.1007/s12221-021-0460-9>
- Rangappa SM, Siengchin S, Parameswaranpillai J et al (2022) Lignocellulosic fiber reinforced composites: Progress, performance, properties, applications, and future perspectives. *Polym Compos* 43:645–691. <https://doi.org/10.1002/pc.26413>
- Mishra R, Wiener J, Militky J et al (2020) Bio-composites reinforced with natural fibers: Comparative analysis of thermal, static and dynamic-mechanical properties. *Fibers Polym* 21:619–627. <https://doi.org/10.1007/s12221-020-9804-0>
- Chua KY, Azzahari AD, Abouloula CN et al (2020) Cellulose-based polymer electrolyte derived from waste coconut husk: residual lignin as a natural plasticizer. *J Polym Res*. <https://doi.org/10.1007/s10965-020-02110-8>
- Dinesh S, Kumaran P, Mohanamurugan S et al (2020) Influence of wood dust fillers on the mechanical, thermal, water absorption and biodegradation characteristics of jute fiber epoxy composites. *J Polym Res*. <https://doi.org/10.1007/s10965-019-1975-2>
- Subash N, Adish Kumar S (2022) A simplified geopolymer concrete mix design considering five mineral admixtures. *Eur J Environ Civ Eng* 26:7572–7585. <https://doi.org/10.1080/19648189.2021.2003252>
- Esfandiari A (2008) The statistical investigation of mechanical properties of PP/natural fibers composites. *Fibers and Polymers* 9:48–54. <https://doi.org/10.1007/s12221-008-0008-2>
- Shih YF, Huang CC (2011) Polylactic acid (PLA)/banana fiber (BF) biodegradable green composites. *J Polym Res* 18:2335–2340. <https://doi.org/10.1007/s10965-011-9646-y>

10. Maurya AK, Manik G (2023) Advances towards development of industrially relevant short natural fiber reinforced and hybridized polypropylene composites for various industrial applications: a review. *J Polym Res* 2022 30:1–20. <https://doi.org/10.1007/S10965-022-03413-8>
11. Mahmud S, Hasan KMF, Jahid MA et al (2021) Comprehensive review on plant fiber-reinforced polymeric biocomposites. Springer, US
12. Asyraf MRM, Syamsir A, Ishak MR et al (2023) Mechanical properties of hybrid lignocellulosic fiber-reinforced biopolymer green composites: a review. *Fibers Polym* 24:337–353. <https://doi.org/10.1007/s12221-023-00034-w>
13. Bhandari K, Roy Maulik S, Bhattacharyya AR (2020) Synthesis and characterization of microcrystalline cellulose from rice husk. *J Inst Eng (India): Ser E* 101:99–108. <https://doi.org/10.1007/s40034-020-00160-7>
14. John MJ, Anandjiwala RD (2008) Recent developments in chemical modification and characterization of natural fiber-reinforced composites. *Polym Compos* 29:187–207. <https://doi.org/10.1002/PC.20461>
15. Kumar M, Revathi K, Khanna S (2015) Biodegradation of cellulosic and lignocellulosic waste by *Pseudoxanthomonas* sp R-28. *Carbohydr Polym* 134:761–766. <https://doi.org/10.1016/j.carbpol.2015.08.072>
16. Subash N, Avudaiappan S, Kumar SA et al (2021) Experimental investigation on geopolymer concrete with various sustainable mineral ashes. *Materials*. <https://doi.org/10.3390/ma14247596>
17. Prakash O, Naik M, Katiyar R et al (2018) Novel process for isolation of major bio-polymers from *Mentha arvensis* distilled biomass and saccharification of the isolated cellulose to glucose. *Ind Crops Prod* 119:1–8. <https://doi.org/10.1016/j.indcrop.2018.03.063>
18. Sunesh NP, Suyambulingam I, Divakaran D, Siengchin S (2023) Isolation of microcrystalline cellulose from *Valoniopsis pachynema* green macroalgae: Physicochemical, thermal, morphological, and mechanical characterization for biofilm applications. *Waste Biomass Valorization*. <https://doi.org/10.1007/s12649-023-02228-y>
19. Narayana Perumal S, Suyambulingam I, Divakaran D, Siengchin S (2023) Extraction and physico-mechanical and thermal characterization of a novel green bio-plasticizer from *Petalium murex* plant biomass for biofilm application. *J Polym Environ*. <https://doi.org/10.1007/s10924-023-02898-8>
20. Hasanin MS, Kassem N, Hassan ML (2021) Preparation and characterization of microcrystalline cellulose from olive stones. *Biomass Convers Biorefin*. <https://doi.org/10.1007/s13399-021-01423-y>
21. Mysiukiewicz O, Sałasińska K, Barczewski M, Szulc J (2020) The influence of oil content within lignocellulosic filler on thermal degradation kinetics and flammability of polylactide composites modified with linseed cake. *Polym Compos* 41:4503–4513. <https://doi.org/10.1002/PC.25727>
22. Barman A, Shrivastava NK, Khatua BB, Ray BC (2015) Green composites based on high-density polyethylene and *Saccharum spontaneum*: Effect of filler content on morphology, thermal, and mechanical properties. *Polym Compos* 36:2157–2166. <https://doi.org/10.1002/PC.23126>
23. Moutousidis D, Karidi K, Athanassiadou E et al (2023) Reinforcement of urea formaldehyde resins with pectins derived from orange peel residues for the production of wood-based panels. *Sustain Chem Environ* 4:100037. <https://doi.org/10.1016/j.scenv.2023.100037>
24. Tarchoun AF, Trache D, Klapötke TM (2019) Microcrystalline cellulose from *Posidonia oceanica* brown algae: Extraction and characterization. *Int J Biol Macromol* 138:837–845. <https://doi.org/10.1016/j.ijbiomac.2019.07.176>
25. Beroual M, Trache D, Mehelli O et al (2021) Effect of the delignification process on the physicochemical properties and thermal stability of microcrystalline cellulose extracted from date palm fronds. *Waste Biomass Valorization* 12:2779–2793. <https://doi.org/10.1007/s12649-020-01198-9>
26. Haque S, Chowdhury A, Rana A et al (2015) Synthesis of microcrystalline cellulose from pretreated cotton obtained from *Bombax ceiba* L. and its characterization. *Bangladesh J Sci Ind Res* 50:199–204. <https://doi.org/10.3329/bjsir.v50i3.25586>
27. Aldosari OF, Jabli M, Morad MH (2023) Chemical extraction of cellulose from Ligno-cellulosic *Astragalus armatus* pods: Characterization, and application to the biosorption of methylene blue. *Arab J Chem*. <https://doi.org/10.1016/j.arabjc.2023.105019>
28. Ventura-Cruz S, Flores-Alamo N, Tecante A (2020) Preparation of microcrystalline cellulose from residual Rose stems (*Rosa* spp.) by successive delignification with alkaline hydrogen peroxide. *Int J Biol Macromol* 155:324–329. <https://doi.org/10.1016/j.ijbiomac.2020.03.222>
29. Somasundaram R, Rajamoni R, Suyambulingam I et al (2022) Utilization of discarded *Cymbopogon flexuosus* root waste as a novel lignocellulosic fiber for lightweight polymer composite application. *Polym Compos* 43:1–16. <https://doi.org/10.1002/pc.26580>
30. Sarala R (2020) Characterization of a new natural cellulosic fiber extracted from *Derris scandens* stem. *Int J Biol Macromol* 165:2303–2313. <https://doi.org/10.1016/j.ijbiomac.2020.10.086>
31. Chandrasekaran NK, Arunachalam V (2021) State-of-the-art review on honeycomb sandwich composite structures with an emphasis on filler materials. *Polym Compos* 42:5011–5020. <https://doi.org/10.1002/PC.26252>
32. Ahmadi M, Madadlou A, Sabouri AA (2015) Isolation of micro- and nano-crystalline cellulose particles and fabrication of crystalline particles-loaded whey protein cold-set gel. *Food Chem* 174:97–103. <https://doi.org/10.1016/j.foodchem.2014.11.038>
33. Alle M, Bandi R, Lee SH, Kim JC (2020) Recent trends in isolation of cellulose nanocrystals and nanofibrils from various forest wood and nonwood products and their application. *Nanomater Agric For Appl Elsevier*, pp 41–80
34. Gabriel T, Belete A, Syrowatka F et al (2020) Extraction and characterization of celluloses from various plant byproducts. *Int J Biol Macromol* 158:1248–1258. <https://doi.org/10.1016/j.ijbiomac.2020.04.264>
35. Haldar D, Purkait MK (2020) Micro and nanocrystalline cellulose derivatives of lignocellulosic biomass: A review on synthesis, applications and advancements. *Carbohydr Polym* 250:116937. <https://doi.org/10.1016/j.carbpol.2020.116937>
36. Hafid HS, Omar FN, Zhu J, Wakisaka M (2021) Enhanced crystallinity and thermal properties of cellulose from rice husk using acid hydrolysis treatment. *Carbohydr Polym*. <https://doi.org/10.1016/j.carbpol.2021.117789>
37. Harini K, Ramya K, Sukumar M (2018) Extraction of nano cellulose fibers from the banana peel and bract for production of acetyl and lauroyl cellulose. *Carbohydr Polym* 201:329–339. <https://doi.org/10.1016/j.carbpol.2018.08.081>
38. Harini K, Chandra Mohan C (2020) Isolation and characterization of micro and nanocrystalline cellulose fibers from the walnut shell, corncob and sugarcane bagasse. *Int J Biol Macromol* 163:1375–1383. <https://doi.org/10.1016/j.ijbiomac.2020.07.239>
39. Kian LK, Saba N, Jawaid M, Fouad H (2020) Characterization of microcrystalline cellulose extracted from olive fiber. *Int J Biol Macromol* 156:347–353. <https://doi.org/10.1016/j.ijbiomac.2020.04.015>
40. Shanmugarajah B, Chew IML, Mubarak NM et al (2019) Valorization of palm oil agro-waste into cellulose biosorbents for highly effective textile effluent remediation. *J Clean Prod* 210:697–709. <https://doi.org/10.1016/j.jclepro.2018.10.342>

41. Rahman MS, Mondal MIH, Yeasmin MS et al (2020) Conversion of lignocellulosic corn agro-waste into cellulose derivative and its potential application as pharmaceutical excipient. Processes. <https://doi.org/10.3390/PR8060711>
42. Ganguly P, Sengupta S, Das P, Bhowal A (2020) Valorization of food waste: Extraction of cellulose, lignin and their application in energy use and water treatment. Fuel 280:118581. <https://doi.org/10.1016/j.fuel.2020.118581>
43. Thomas SK, Parameswaranpillai J, Krishnasamy S et al (2021) A comprehensive review on cellulose, chitin, and starch as fillers in natural rubber biocomposites. Carbohydr Polym Technol Appl 2:100095. <https://doi.org/10.1016/j.carpta.2021.100095>
44. Van NTT, Gaspillo PA, Thanh HG et al (2022) Cellulose from the banana stem: optimization of extraction by response surface methodology (RSM) and characterization. Heliyon. <https://doi.org/10.1016/j.heliyon.2022.e11845>
45. Fouad H, Kian LK, Jawaid M et al (2020) Characterization of microcrystalline cellulose isolated from conocarpus fiber. Polymers (Basel) 12:1–11. <https://doi.org/10.3390/polym12122926>
46. Kalpana VP, Perarasu VT (2020) Analysis on cellulose extraction from hybrid biomass for improved crystallinity. J Mol Struct 1217:128350. <https://doi.org/10.1016/j.molstruc.2020.128350>
47. Sainorudin MH, Mohammad M, Kadir NHA et al (2018) Characterization of several microcrystalline cellulose (Mcc)-based agricultural wastes via x-ray diffraction method. Solid State Phenomena 280(SSP):340–345. <https://doi.org/10.4028/www.scientific.net/SSP.280.340>
48. Suyambulingam I, Divakaran D, Siengchin S (2023) Comprehensive characterization of novel Borassus flabellifer flower biomass based microcrystalline cellulose reinforced with polylactic acid (PLA) biofilm for futuristic applications. Biomass Convers Biorefin. <https://doi.org/10.1007/s13399-023-04030-1>
49. Divakaran D, Suyambulingam I, Sanjay MR et al (2024) International Journal of Biological Macromolecules Isolation and characterization of microcrystalline cellulose from an agro-waste tamarind (Tamarindus indica) seeds and its suitability investigation for biofilm formulation. Int J Biol Macromol 254:127687. <https://doi.org/10.1016/j.ijbiomac.2023.127687>
50. Ranthesh J, Indran S, Raja S et al (2023) Isolation and characterization of novel micro cellulose from *Azadirachta indica* A. Juss agro-industrial residual waste oil cake for futuristic applications. Biomass Conv Bioref 13:4393–4411. <https://doi.org/10.1007/s13399-022-03467-0>
51. Baruah J, Deka RC, Kalita E (2020) Greener production of microcrystalline cellulose (MCC) from Saccharum spontaneum (Kans grass): Statistical optimization. Int J Biol Macromol 154:672–682. <https://doi.org/10.1016/j.ijbiomac.2020.03.158>
52. Nabili A, Fattoum A, Passas R, Elaloui E (2016) Extraction and characterization of cellulose from date palm seeds (*Phoenix dactylifera* L.). Cellul Chem Technol 50:1015–1023
53. Xiao W, Niu B, Yu M et al (2021) Fabrication of foam-like oil sorbent from polylactic acid and *Calotropis gigantea* fiber for effective oil absorption. J Clean Prod 278:123507. <https://doi.org/10.1016/j.jclepro.2020.123507>
54. Athirah Abdullah N, Hanif Sainorudin M, Asim N et al (2020) Extraction of microcrystalline cellulose from two different agriculture waste via chemical treatment. IOP Conf Ser Mater Sci Eng. <https://doi.org/10.1088/1757-899X/739/1/012017>
55. Sivamurugan P, Selvam R, Pandian M et al (2022) Extraction of novel biosilica from finger millet husk and its coconut rachilla-reinforced epoxy biocomposite: mechanical, thermal, and hydrophobic behaviour. Biomass Convers Biorefin. <https://doi.org/10.1007/s13399-022-03342-y>
56. Sumesh KR, Kavimani V, Rajeshkumar G et al (2022) Mechanical, water absorption and wear characteristics of novel polymeric composites: Impact of hybrid natural fibers and oil cake filler addition. J Ind Text 51:5910S–5937S
57. Igathinathane C, Pordesimo LO, Columbus EP et al (2009) Sieveless particle size distribution analysis of particulate materials through computer vision. Comput Electron Agric 66:147–158. <https://doi.org/10.1016/j.compag.2009.01.005>
58. Collazo-Bigliardi S, Ortega-Toro R, Chiralt Boix A (2018) Isolation and characterisation of microcrystalline cellulose and cellulose nanocrystals from coffee husk and comparative study with rice husk. Carbohydr Polym 191:205–215. <https://doi.org/10.1016/j.carbpol.2018.03.022>
59. Queirós CSGP, Cardoso S, Lourenço A et al (2020) Characterization of walnut, almond, and pine nut shells regarding chemical composition and extract composition. Biomass Convers Biorefin 10:175–188. <https://doi.org/10.1007/s13399-019-00424-2>
60. Senthil Muthu Kumar T, Rajini N, Obi Reddy K et al (2018) All-cellulose composite films with cellulose matrix and Napier grass cellulose fibril fillers. Int J Biol Macromol 112:1310–1315. <https://doi.org/10.1016/j.ijbiomac.2018.01.167>
61. Reddy KO, Uma Maheswari C, Muzenda E et al (2016) Extraction and characterization of cellulose from pretreated ficus (peepal tree) leaf fibers. J Nat Fibers 13:54–64. <https://doi.org/10.1080/15440478.2014.984055>
62. de Moreira BR, A, Cruz VH, Barbosa Júnior MR, et al (2022) Agro-residual biomass and disposable protective face mask: a merger for converting waste to plastic-fiber fuel via an integrative carbonization-pelletization framework. Biomass Convers Biorefin. <https://doi.org/10.1007/s13399-022-03285-4>
63. Narayanasamy P, Balasundar P, Senthil S et al (2020) Characterization of a novel natural cellulosic fiber from *Calotropis gigantea* fruit bunch for ecofriendly polymer composites. Int J Biol Macromol 150:793–801. <https://doi.org/10.1016/j.ijbiomac.2020.02.134>
64. Moreno G, Ramirez K, Esquivel M, Jimenez G (2019) Biocomposite films of polylactic acid reinforced with microcrystalline cellulose from pineapple leaf fibers. J Renew Mater 7:9–20. <https://doi.org/10.32604/jrm.2019.00017>
65. Katakajwala R, Mohan SV (2020) Microcrystalline cellulose production from sugarcane bagasse: Sustainable process development and life cycle assessment. J Clean Prod 249:119342. <https://doi.org/10.1016/j.jclepro.2019.119342>
66. Ilyas RA, Sapuan SM, Ibrahim R et al (2019) Effect of sugar palm nanofibrillated cellulose concentrations on morphological, mechanical and physical properties of biodegradable films based on agro-waste sugar palm (*Arenga pinnata* (Wurmb.) Merr) starch. J Market Res 8:4819–4830. <https://doi.org/10.1016/j.jmrt.2019.08.028>
67. Bhandari K, Roy P, Bhattacharyya AR, Maulik SR (2020) Synthesis and characterization of microcrystalline cellulose from jute stick. Indian J Fibre Text Res 45:464–469. <https://doi.org/10.56042/ijfr.v45i4.30460>
68. Siddhanta AK, Prasad K, Meena R et al (2009) Profiling of cellulose content in Indian seaweed species. Bioresour Technol 100:6669–6673. <https://doi.org/10.1016/j.biortech.2009.07.047>
69. Sun X, Lu C, Liu Y et al (2014) Melt-processed poly (vinyl alcohol) composites filled with microcrystalline cellulose from waste cotton fabrics. Carbohydr Polym 101:642–649
70. Pinheiro Bruni G, de Oliveira JP, Gómez-Mascaraque LG et al (2020) Electrospun β -carotene-loaded SPI/PVA fiber mats produced by emulsion-electrospinning as bioactive coatings for food packaging. Food Packag Shelf Life 23:100426. <https://doi.org/10.1016/j.fpsl.2019.100426>
71. Rajashekar V, Rao EU, Srinivas P (2012) Biological activities and medicinal properties of Gokhru (*Pedalium murex* L.). Asian Pac J Trop Biomed 2:581–585. [https://doi.org/10.1016/S2221-1691\(12\)60101-4](https://doi.org/10.1016/S2221-1691(12)60101-4)

72. Cao Y, Zandi Y, Rahimi A et al (2021) A new intelligence fuzzy-based hybrid metaheuristic algorithm for analyzing the application of tea waste in concrete as natural fiber. *Comput Electron Agric*. <https://doi.org/10.1016/j.compag.2021.106420>
73. Adel AM, Abd El-Wahab ZH, Ibrahim AA, Al-Shemy MT (2011) Characterization of microcrystalline cellulose prepared from lignocellulosic materials. Part II: Physicochemical properties *Carbohydr Polym* 83:676–687. <https://doi.org/10.1016/j.carbpol.2010.08.039>
74. Beroual M, Boumaza L, Mehelli O et al (2021) Physicochemical properties and thermal stability of microcrystalline cellulose isolated from esparto grass using different delignification approaches. *J Polym Environ* 29:130–142. <https://doi.org/10.1007/s10924-020-01858-w>
75. Thilagashanthi T, Gunasekaran K, Satyanarayanan KS (2021) Microstructural pore analysis using SEM and ImageJ on the absorption of treated coconut shell aggregate. *J Clean Prod* 324:129217. <https://doi.org/10.1016/j.jclepro.2021.129217>
76. Sarmin SN, Jawaid M, Mahmoud MH et al (2022) Mechanical and physical properties analysis of olive biomass and bamboo reinforced epoxy-based hybrid composites. *Biomass Convers Biorefin*. <https://doi.org/10.1007/s13399-022-02872-9>
77. Kalita RD, Nath Y, Ochubiojo ME, Buragohain AK (2013) Extraction and characterization of microcrystalline cellulose from fodder grass; *Setaria glauca* (L) P. Beauv, and its potential as a drug delivery vehicle for isoniazid, a first line antituberculosis drug. *Colloids Surf B Biointerfaces* 108:85–89
78. Baruah J, Bardhan P, Mukherjee AK et al (2022) Integrated pretreatment of banana agrowastes: Structural characterization and enhancement of enzymatic hydrolysis of cellulose obtained from banana peduncle. *Int J Biol Macromol* 201:298–307. <https://doi.org/10.1016/j.ijbiomac.2021.12.179>
79. Hamdan MA, Ramli NA, Othman NA et al (2019) Characterization and property investigation of microcrystalline cellulose (MCC) and carboxymethyl cellulose (CMC) filler on the carrageenan-based biocomposite film. *Mater Today Proc* 42:56–62. <https://doi.org/10.1016/j.matpr.2020.09.304>
80. Thiangtham S, Runt J, Saito N, Manuapiya H (2020) Fabrication of biocomposite membrane with microcrystalline cellulose (MCC) extracted from sugarcane bagasse by phase inversion method. *Cellulose* 27:1367–1384. <https://doi.org/10.1007/s10570-019-02866-3>
81. Nagarajan KJ, Balaji AN, Basha KS et al (2020) Effect of agro waste α -cellulosic micro filler on mechanical and thermal behavior of epoxy composites. *Int J Biol Macromol* 152:327–339. <https://doi.org/10.1016/j.ijbiomac.2020.02.255>
82. Tarchoun AF, Trache D, Klapötke TM et al (2019) Ecofriendly isolation and characterization of microcrystalline cellulose from giant reed using various acidic media. *Cellulose* 26:7635–7651. <https://doi.org/10.1007/s10570-019-02672-x>
83. Joe MS, Sudherson DPS, Suyambulingam I et al (2023) Extraction and characterization of novel biomass-based cellulosic plant fiber from *Ficus benjamina* L. stem for a potential polymeric composite reinforcement. *Biomass Conv Bioref* 13:14225–14239. <https://doi.org/10.1007/s13399-023-03759-z>
84. Sunesh NP, Indran S, Divya D, Suchart S (2022) Isolation and characterization of novel agrowaste-based cellulosic micro fillers from *Borassus flabellifer* flower for polymer composite reinforcement. *Polym Compos* 43:6476–6488
85. Porzio L, Arena C, Lorenti M et al (2020) Long-term response of *Diclytota dichotoma* var. *intricata* (C, Agardh) Greville (Phaeophyceae) to ocean acidification: Insights from high pCO₂ vents. *Sci Total Environ* 731:138896. <https://doi.org/10.1016/j.scitotenv.2020.138896>
86. Divakaran D, Suyambulingam I, Sanjay MR et al (2024) Isolation and characterization of microcrystalline cellulose from an agro-waste tamarind (*Tamarindus indica*) seeds and its suitability investigation for biofilm formulation. *Int J Biol Macromol* 254:127687. <https://doi.org/10.1016/j.ijbiomac.2023.127687>
87. Asem M, Nawawi WMFW, Jimat DN (2018) Evaluation of water absorption of polyvinyl alcohol-starch biocomposite reinforced with sugarcane bagasse nanofibre: Optimization using Two-Level Factorial Design. *IOP Conf Ser Mater Sci Eng*. <https://doi.org/10.1088/1757-899X/368/1/012005>
88. Zhao T, Chen Z, Lin X et al (2018) Preparation and characterization of microcrystalline cellulose (MCC) from tea waste. *Carbohydr Polym* 184:164–170. <https://doi.org/10.1016/j.carbpol.2017.12.024>
89. Dastjerdi S, Naeijian F, Akgöz B, Civalek Ö (2021) On the mechanical analysis of microcrystalline cellulose sheets. *Int J Eng Sci* 166:103500. <https://doi.org/10.1016/j.ijengsci.2021.103500>
90. Atabaki F, Bastam NN, Hafizi-Atabak HR et al (2020) Synthesis and characterization of new energetic plasticizers: Benzoyl-terminated poly(epichlorohydrin) modified by phenylhydrazine and its derivatives. *Cent Eur J Energ Mater* 17:323–343. <https://doi.org/10.22211/cejem/127514>
91. Ibáñez-García A, Martínez-García A, Ferrándiz-Bou S (2021) Influence of almond shell content and particle size on mechanical properties of starch-based biocomposites. *Waste Biomass Valorization* 12:5823–5836. <https://doi.org/10.1007/s12649-020-01330-9>
92. Sanjeewa KKA, Kang N, Ahn G et al (2018) Bioactive potentials of sulfated polysaccharides isolated from brown seaweed *Sargassum* spp in related to human health applications: A review. *Food Hydrocoll* 81:200–208. <https://doi.org/10.1016/j.foodhyd.2018.02.040>
93. Renugadevi K, Devan PK, Thomas T (2019) Fabrication of Calotropis Gigantea fibre reinforced compression spring for light weight applications. *Compos B Eng* 172:281–289. <https://doi.org/10.1016/j.compositesb.2019.05.037>
94. Chen B, Li L, Hu Y et al (2022) Fluorescence turn-on immunoassay of endocrine diethyl phthalate in daily supplies using red fluorescent carbon dots. *Microchem J* 178:107350. <https://doi.org/10.1016/j.microc.2022.107350>
95. Pracella M, Haque MMU, Puglia D (2014) Morphology and properties tuning of PLA/cellulose nanocrystals bio-nanocomposites by means of reactive functionalization and blending with PVAc. *Polymer (Guildf)* 55:3720–3728. <https://doi.org/10.1016/j.polymer.2014.06.071>
96. Sturm DJ, Bachner J, Renninger D et al (2021) Corrigendum to “A cluster randomized trial to evaluate need-supportive teaching in physical education on physical activity of sixth-grade girls: A mixed method study” [Psychology of Sport & Exercise 54 (2021) 101902] (Psychology of Sport & Exercise (2021). *Psychol Sport Exerc* 57:102035. <https://doi.org/10.1016/j.psychsport.2021.102035>
97. Xiao X, Lu S, Qi B et al (2014) Enhancing the thermal and mechanical properties of epoxy resins by addition of a hyperbranched aromatic polyamide grown on microcrystalline cellulose fibers. *RSC Adv* 4:14928–14935
98. Trivedi N, Gupta V, Kumar M et al (2011) An alkali-halotolerant cellulase from *Bacillus flexus* isolated from green seaweed *Ulva lactuca*. *Carbohydr Polym* 83:891–897. <https://doi.org/10.1016/j.carbpol.2010.08.069>
99. Lu JH, Chen C, Huang C, Lee DJ (2020) Glucose fermentation with biochar-amended consortium: microbial consortium shift. *Bioengineered* 11:272–280. <https://doi.org/10.1080/21655979.2020.1735668>

Publisher's Note Springer Nature remains neutral with regard to jurisdictional claims in published maps and institutional affiliations.

Springer Nature or its licensor (e.g. a society or other partner) holds exclusive rights to this article under a publishing agreement with the author(s) or other rightsholder(s); author self-archiving of the accepted manuscript version of this article is solely governed by the terms of such publishing agreement and applicable law.